Substrate Binding and Catalytic Mechanism of Human Choline Acetyltransferase[†,‡]

Ae-Ri Kim,[§] R. Jane Rylett,*[,||,⊥] and Brian H. Shilton*[,§]

Department of Biochemistry, and Physiology and Pharmacology, Schulich School of Medicine and Dentistry, University of Western Ontario, and Cell Biology Research Group, Robarts Research Institute, London, Ontario, Canada

Received July 30, 2006; Revised Manuscript Received October 1, 2006

ABSTRACT: Choline acetyltransferase (ChAT) catalyzes the synthesis of the neurotransmitter acetylcholine from choline and acetyl-CoA, and its presence is a defining feature of cholinergic neurons. We report the structure of human ChAT to a resolution of 2.2 Å along with structures for binary complexes of ChAT with choline, CoA, and a nonhydrolyzable acetyl-CoA analogue, *S*-(2-oxopropyl)-CoA. The ChAT−choline complex shows which features of choline are important for binding and explains how modifications of the choline trimethylammonium group can be tolerated by the enzyme. A detailed model of the ternary Michaelis complex fully supports the direct transfer of the acetyl group from acetyl-CoA to choline through a mechanism similar to that seen in the serine hydrolases for the formation of an acyl−enzyme intermediate. Domain movements accompany CoA binding, and a surface loop, which is disordered in the unliganded enzyme, becomes localized and binds directly to the phosphates of CoA, stabilizing the complex. Interactions between this surface loop and CoA may function to lower the K_M for CoA and could be important for phosphorylation-dependent regulation of ChAT activity.

Choline acetyltransferase (ChAT[1], E.C. 2.3.1.6) catalyzes the transfer of an acetyl group from acetyl-CoA to choline to form the neurotransmitter acetylcholine. Communication between cholinergic neurons and their target cells and tissues is dependent on functional ChAT, with the loss of ChAT expression and activity found in several neurological and psychiatric disorders, such as Alzheimer's disease (*1*), schizophrenia (*2*), and neuromuscular diseases (*3*). Although primarily associated with the cholinergic nervous system, both ChAT and acetylcholine are also found in cells and tissues such as T-lymphocytes (*4*) and placenta (*5*), suggesting that acetylcholine may have a novel role in non-neuronal systems.

ChAT is a relatively large, complex protein that is produced from six different mRNAs, termed H-, M-, N1-, N2-, R-, and S-ChAT; two of these transcripts, M- and S-ChAT, also encode 83- and 74-kDa forms of the protein through alternative translation start sites. Interestingly, human ChAT (hChAT) has functional nuclear localization signal motifs that are involved in regulating its distribution between the nucleus and cytoplasm (*6*, *7*); furthermore, it has been demonstrated recently that ChAT is present in the nuclei of cholinergic neurons in necropsy human brain and spinal cord (*8*). Although a functional role for ChAT in neuronal nuclei has not been identified, polymorphism in its transcripts and the targeting of the enzyme to the nucleus suggests that ChAT may engage in more complex functions in addition to its essential role synthesizing acetylcholine in nerve termini.

To serve its function as a neurotransmitter, the acetylcholine synthesized by ChAT must be transported into synaptic vesicles by the vesicular acetylcholine transporter (*9*). Acetylcholine is base-labile, but an acidic pH is maintained inside the vesicles, providing an optimal environment for the temporary storage of acetylcholine. To minimize the time between synthesis and storage and to facilitate uptake by the vesicular acetylcholine transporter, acetylcholine synthesis may be localized to the immediate vicinity of the synaptic vesicles. Most of the choline used for acetylcholine synthesis is obtained from the extracellular compartment (*10*) via the plasma membrane high-affinity choline transporter (*11*), and therefore, acetylcholine synthesis must take place next to this choline transporter. Both ChAT and the choline transporter can be associated with synaptic vesicles (*12*, *13*). The binding of ChAT to membranes and its co-localization with the two transporters would facilitate both the use of choline obtained from the extracellular compartment and the accumulation of newly synthesized acetylcholine into synaptic vesicles. Although it is not fully understood how the membrane association of ChAT is controlled and the degree to which its catalytic activity is regulated, recent studies suggest that the phosphorylation of ChAT may play a role in both its activity and subcellular localization (*14*).

[†] This work was supported by Canadian Institutes of Health Research (CIHR) Grant MOP-44005 to R.J.R. and B.H.S. Data collection at beamline X8C was supported by a CIHR multiuser grant and Natural Sciences and Engineering Research Council major facilities access grant.

[‡] Crystal structure coordinates have been deposited in the Protein Data Bank with codes 2FY2, 2FY3, 2FY4, and 2FY5.

* To whom correspondence should be addressed. Phone: 519-661-4124. Fax 519-661-3175. E-mail: bshilton@uwo.ca (B.H.S.). Phone: 519-663-5777 x34078. Fax: 519-663-3314. E-mail: jane.rylett@schulich.uwo.ca (R.J.R.).

[§] Department of Biochemistry, University of Western Ontario.

[||] Physiology and Pharmacology, University of Western Ontario.

[⊥] Robarts Research Institute.

[1] Abbreviations: BPTI, bovine pancreatic trypsin inhibitor; ChAT, choline acetyltransferase; CoA, coenzyme-A; CrAT, carnitine acetyltransferase; HC-3, hemicholinium-3; hChAT, human ChAT; PDB, Protein Data Bank; PEG, polyethylene glycol; PKC, protein kinase C; rChAT, rat ChAT; RMSD, root mean square distance; TCEP, tris(2-carboxyethyl)phosphine.

10.1021/bi061536l CCC: $33.50
Published on Web 11/16/2006

Table 1: Data Collection and Refinement for HChAT Structures

	ChAT	ChAT− choline	ChAT-CoA	ChAT− [*S*-(2-oxopropyl) -CoA]
		crystallographic data		
space group	$P2_12_12_1$	$P2_12_12_1$	$P2_12_12_1$	$P2_12_12_1$
resolution (Å)	2.25	2.25	2.3	2.6
unit-cell parameters (Å)	$a = 54.74$	$a = 54.78$	$a = 54.70$	$a = 55.00$
	$b = 75.75$	$b = 76.26$	$b = 73.98$	$b = 73.93$
	$c = 165.69$	$c = 164.29$	$c = 165.70$	$c = 165.66$
no. of observations	166287	178465	359471	385898
no. of unique reflections	32578	29676	30048	19670
$I/\sigma I$[a]	17.1 (9.7)	7.0 (2.8)	6.7 (2.7)	6.2 (1.8)
R_{merge}[a]	3.8 (9.3)	6.5 (19.8)	8.0 (28.8)	13.3 (53.0)
completeness[a,b] (%)	94.3 (90.4)	84.0 (42.9)	93.1 (85.6)	83.7 (57.7)
		refinement statistics		
R_{work}/ R_{free}	0.195/0.235	0.196/0.233	0.203/0.240	0.237/0.280
no. protein atoms	4584	4653	4604	4514
no. solvent molecules	544	546	447	104
average B values (Å^2)	19.3	22.1	29.4	43.6
protein	18.2	21.5	29.2	43.6
solvent	28.5	27.6	31.5	37.3
ligand		22.3	29.0	50.1
rmsd bond lengths	0.007	0.006	0.009	0.007
rmsd bond angles	1.3	1.2	1.4	1.3
pdb ID	2FY2	2FY3	2FY4	2FY5

[a] Values in parentheses correspond to the highest resolution shell. [b] For reflections with $I > \sigma I$.

ChAT is a member of the CoA-dependent acyltransferase superfamily that includes carnitine acetyltransferase, chloramphenicol acetyltransferase, dihydrolipoyl transacetylase, and VibH (*15*). In all members of the family, the active site is buried in the interface between two domains and is accessible to substrates through tunnels on either side of the enzyme. Results from kinetic studies indicate that synthesis of acetylcholine by ChAT follows an ordered sequential reaction in which the acetyl group is transferred directly to choline from acetyl-CoA, with acetyl-CoA being the leading substrate (*16*). An essential histidine residue, corresponding to H324 in hChAT (*17*), is thought to act as a general base catalyst in the reaction. The activity of ChAT is decreased under oxidizing conditions and by modification with sulfhydryl-reactive agents (*18*), indicating the presence of cysteines in the vicinity of the active site. Reaction of ChAT with butanedione, an arginine-modifying reagent, affects the activity of the enzyme (*19*), and two arginine residues, R442 and R443, have been shown to be involved in CoA binding (*20*). In addition to these arginine residues, the binding of acetyl-CoA and CoA are strongly affected by the enzyme's environment: the dissociation of CoA is the rate-limiting step at low ionic strength, but other steps become rate-limiting at high ionic strength (*21*, *22*). The effect of ionic strength is not evident with dephospho-CoA, and therefore it is thought that anions compete for the 3′-phosphate binding site (*20*).

Crystal structures of unliganded rat ChAT (rChAT) have been published (*23*, *24*), and these structures include a description of an unrefined 3.7 Å resolution rChAT-CoA structure (*23*) and a model for the rChAT-choline complex (*24*), but high-resolution structures of the enzyme in complex with either CoA or choline are not available. A structure for human ChAT (hChAT) was elusive because of the difficulties in obtaining diffraction-quality crystals, but mutation of key surface residues facilitated rapid, reproducible crystallization (*25*), allowing us to obtain high-resolution structures for hChAT alone and in complex with its ligands. These structures provide a comprehensive description of CoA and choline binding along with insight into the catalytic mechanism for human ChAT.

RESULTS AND DISCUSSION

Structure of HChAT. Crystallization of hChAT was accomplished by the mutation of selected surface residues to reduce conformational entropy (*25*). The surface mutations did not affect the catalytic properties of hChAT (*25*), but they did make the enzyme extremely easy to crystallize, thereby facilitating a comprehensive structural analysis of the apo form and binary complexes with choline, CoA, and *S*-(2-oxopropyl)-CoA, a stable acetyl-CoA analogue. Data collection and refinement statistics for unliganded ChAT and the three complexes are given in Table 1. The structure of unliganded hChAT was solved by molecular replacement using coordinates from the rat enzyme (*23*), and the refined structure of unliganded hChAT is similar to that of the rat enzyme, with an rmsd (CA positions) of 0.72 Å (Figure 1A).

HChAT is composed of two domains, each consisting of a six-stranded β-sheet surrounded by α-helices, with the same pseudo 2-fold symmetry noted originally for the related carnitine acetyltransferase (*26*). The active site histidine, H324 (*17*), is at the interface between these two domains, in the middle of a tunnel that runs through the enzyme (Figure 1B). The domains can be defined on the basis of their function. The binding domain includes residues 1 to 89 and 392 to 615 and makes most of the interactions with the two substrates, CoA and choline, as will be evident from the structures of the binary complexes. The catalytic domain consists of residues 90 to 391 and contains H324 and other residues that are important for catalysis.

An inspection of crystal-packing interactions shows that engineered surface residues mediated two crystal contacts. One of the crystal contacts involved E225A, D226A, and E227A on one molecule and residues H134 and Y156 on a symmetry-related molecule (Figure 2A). The other included

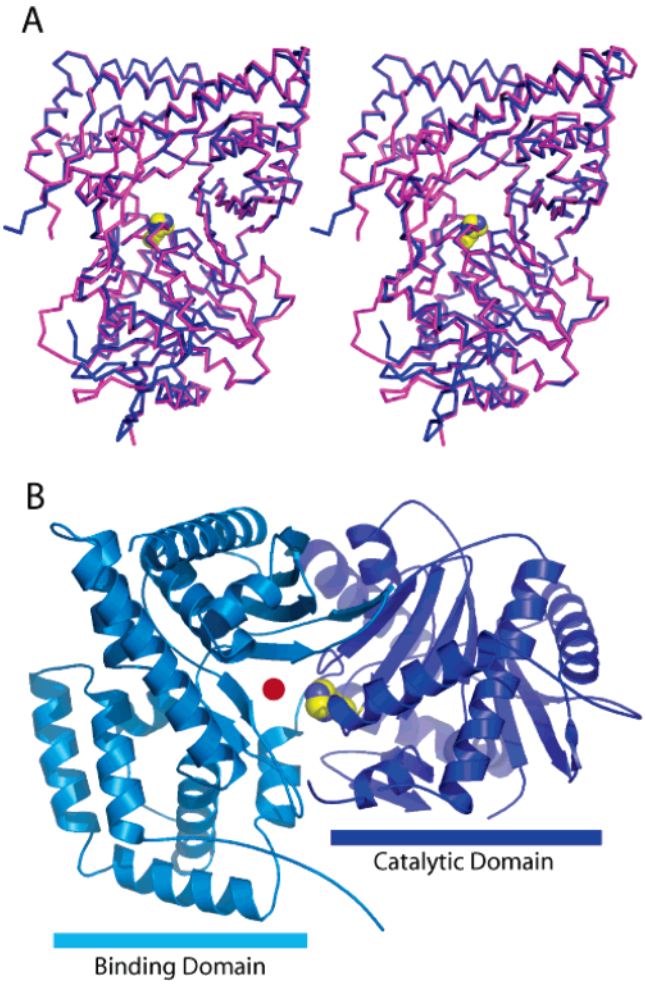

FIGURE 1: Domain structure of HChAT and comparison to rat ChAT. (A) CA backbone traces of the rat enzyme (magenta; pdb accession code 1Q6X; *23*) superimposed on hChAT (blue). The rmsd for CA atoms is 0.72 Å for the superimposed structures. (B) HChAT can be divided into two domains, a substrate binding domain (light blue), comprising residues 1 to 89 and 392 to 615, and a catalytic domain (dark blue), comprising residues 90 to 391. The active site tunnel, which runs through the enzyme and is located at the domain interface, is indicated by the red circle. CoA binds between the two splayed β-strands (on either side of the red circle) at the mouth of the active site tunnel. The side chain of the catalytic histidine, H324, is shown as a space-filling CPK model.

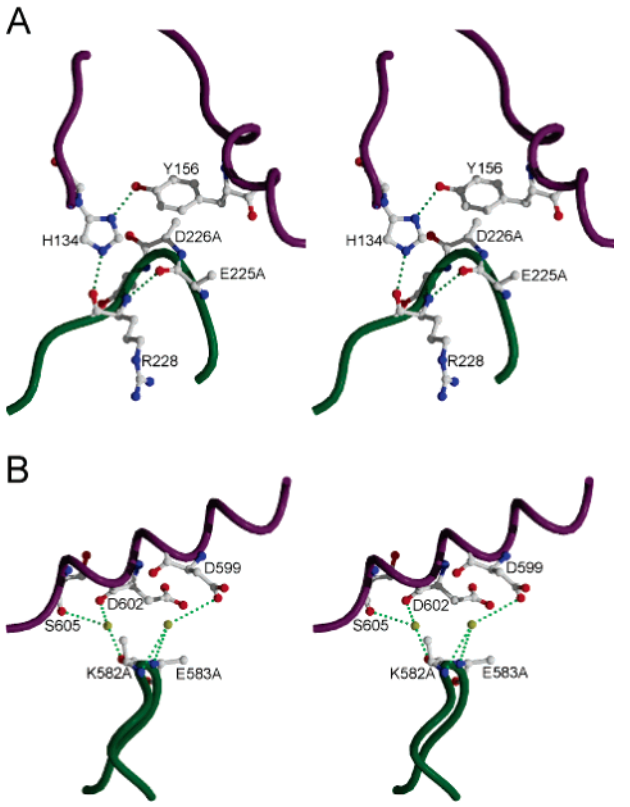

FIGURE 2: Engineered crystal contacts in HChAT. The stereo diagrams illustrate crystal contacts in hChAT that were mediated by surface residues mutated to A from either K, D, or E. (A) The mutations E225A, D226A, and E227A facilitate close contact and hydrogen-bonding interactions (dotted green lines) with H134 and Y156 on a symmetry-related molecule. (B) The mutations K582A and E583A allowed a crystal contact to form via water molecules (yellow spheres) that mediate hydrogen bonds to the C-terminal helix of a symmetry-related molecule.

K582A and E583A and residues D599, D602, and S605 on a symmetry-related molecule (Figure 2B).

Choline Binding. To obtain information on the mode of substrate binding by hChAT, the enzyme was crystallized in the presence of 10 mM acetylcholine. The crystals were isomorphous to unliganded hChAT, and the initial *Fo*−*Fc* difference electron density map (Figure 3A) showed a clear boundary for the choline moiety, including the choline oxygen atom, but absolutely no density that could correspond to the acetyl moiety, even when contoured at 1.5σ. On this basis, we concluded that the acetate ester had been hydrolyzed and that only choline was bound to the enzyme. Choline was positioned using the trimethylammonium group, which was distinguishable as a peak of electron density with three protruding knobs. The trimethylammonium group sits on a ledge against one side of the substrate-binding tunnel; two of the N-linked methyl groups are cradled in form-fitting indentations in this ledge, whereas the third methyl group hangs over the ledge and points toward the exit from the tunnel. In this position, the trimethylammonium group interacts with ChAT through a cation-π bond with the side chain of Y552 and van der Waals interactions with the side chains of M84 and Y436 (Figure 3B). Interactions between the binding domain and the trimethylammonium group function to position the choline hydroxyl such that it is 2.8 Å from the catalytic histidine, H324, and ideally oriented to make a hydrogen bond with NE2 of the H324 imidazole ring. A requirement for the precise positioning of the choline hydroxyl may explain why ChAT is so sensitive to oxidation (*27*). There is a cluster of four cysteine residues in the vicinity of the choline binding site (Figure 3B), and within this cluster, disulfide bonds could form between C563 and C550 or C574, or between C550 and C574 (Figure 3B). Any one of these disulfide bonds would affect the structure of the choline binding site and, in particular, the position of Y552, which is in intimate contact with the choline trimethylammonium group. These cysteines, along with C322, are the only ones in the vicinity of the active site, and one or more of them likely represents the site of modification by sulfhydryl-reactive agents (*18*).

The side chains of S438 and S538, along with the main chain carbonyl of G553, contribute dipoles that impart a net negative electrostatic potential to the trimethylammonium binding surface (Figure 3A). The tunnel leading to the choline binding site also has a negative surface potential, which does not extend to the outside surface of the enzyme

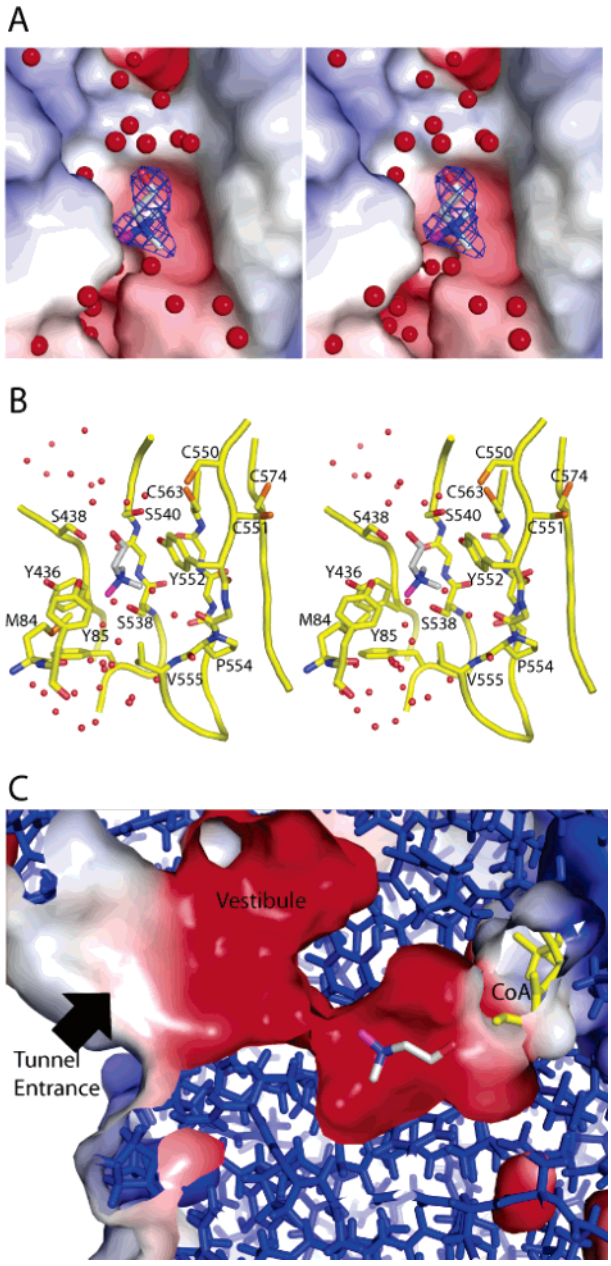

FIGURE 3: Choline binding site of HChAT. HChAT was cocrystallized with acetylcholine, but the initial difference electron density map (blue mesh, contoured at 3σ) showed only the presence of bound choline, indicating that the acetyl group had been hydrolyzed during crystallization. Note that to distinguish between the three trimethylammonium methyl groups, two have been colored white, whereas the third is colored magenta. (A) The choline binding surface is made up of residues belonging to the binding domain and is colored according to its surface potential. Two of the trimethylammonium methyl groups (in white) are cradled on a ledge in the active site tunnel, whereas the third methyl group (in magenta) hangs over this ledge and points toward the exit from the tunnel. Crystallographic waters are indicated by red spheres, showing that there is considerable space around the trimethylammonium group, which explains how the enzyme can accommodate a variety of nitrogen-substituted choline analogues. (B) Specific residues involved in binding choline are illustrated in this stereo diagram. Note that the crystallographic waters at the top of the panel, between S438 and S540, are occupying the space where the pantothiene arm of CoA binds. (C) A cutaway view of the enzyme to show the surface properties of the tunnel in the vicinity of the choline binding site. The surface has been colored according to electrostatic potential. The position of bound choline is shown, and a CoA molecule (yellow atoms; modeled using the binary ChAT-CoA complex) indicates the relative position of the CoA binding site.

Table 2: Chemical Structure of Choline and Analogues

Compound	K_M[a] (mM)	Structure
choline	0.17	
monoethylcholine	1.3	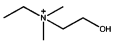
pyrrolcholine	6.7	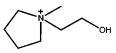
β-methylcholine	N.D.[b]	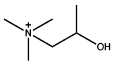
homocholine	N.D.	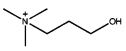
hemicholinium-3 (hemi-acetal)	1.9[c]	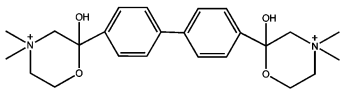
hemicholinium-3 (seco)	N.D.[c]	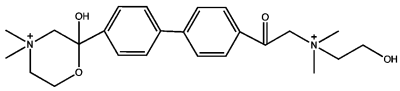

[a] Kinetic parameters were obtained from Barker and Mittag (*28*). [b] At 50 mM, β-methylcholine (D or L isomer) is acetylated at a rate less than 5% that of choline. [c] The K_M for hemicholinium-3 refers to an equilibrium mixture of the hemi-acetal form and seco forms in which the hemi-acetal form is expected to predominate. The seco form is most likely the form that is acetylated.

(Figure 3C). The entrance to the tunnel is much larger than that required to accommodate choline, and there is a vestibule adjacent to the choline binding site with a pronounced negative electrostatic potential. A similar negatively charged vestibule is not present in the homologous carnitine acetyltransferase (*26*), which may reflect the fact that choline is a cation, whereas carnitine is a zwitterion. In ChAT, there is space in the vestibule for an additional choline molecule, but a choline ion was not evident in the electron density, and therefore there does not appear to be a specific choline binding site in the vestibule. The negatively charged vestibule may function to attract choline molecules to the vicinity of the active site and/or facilitate the exchange of choline for acetylcholine at the active site.

The ability of ChAT to interact with and acetylate a number of different choline analogues can be rationalized from the mode of choline binding seen in the ChAT−choline complex. The area around the trimethylammonium group is rather open, as indicated in Figure 3 by the presence of crystallographic waters; in contrast, the α- and β-carbons of choline are sandwiched between the wall of the active site tunnel and the side chains of M84 and Y85 (Figure 3B). These observations explain why the enzyme can accommodate substantial changes to the groups attached to the nitrogen, but not to the α- or β-carbons (*22*, *28*; Table 2). For example, the K_M for α-methylcholine is over 100-fold higher than that for choline, and β-methylcholine is such a poor substrate that the K_M has not been determined. The addition of an extra methylene group in homocholine (Table

2) also has a striking effect because homocholine is not acetylated by soluble ChAT *in vitro* (*29*−*31*). Thus, the separation between the hydroxyl and trimethylammonium groups is critical and is determined by the distance between the ledge on which the trimethylammonium group sits and the catalytic machinery. On this basis, it is interesting that homocholine is acetylated *in situ* by a membrane-associated form of ChAT (*29*). It may be that membrane association leads to a conformational change in the enzyme, perhaps by altering the positions of residues M84 and Y85, thereby providing room for the homocholine methylene carbons to bulge outward and bring the hydroxyl group into the correct position for catalysis. Residues M84 and Y85 are on a coil region connecting the binding domain and the catalytic domain, and therefore it is not unreasonable to think that they could be subject to conformational changes.

In contrast to the α and β carbons, ChAT can accommodate modifications at the choline nitrogen. For example, monoethylcholine has a K_M only 7-fold higher than that of choline, and pyrrolcholine, in which the nitrogen is part of a 5-membered ring, is still a reasonably good substrate (*28*). An intriguing substrate for ChAT is hemicholinium-3 (HC-3), which has a K_M only 10-fold greater than that of choline despite its radically different structure (Table 2). In fact, the open-ring (seco) form, rather than the hemi-acetal, is most likely the molecule that is bound and acetylated by ChAT. As noted by Barker and Mittag (*28*), the seco form "can be viewed as an N-substituted choline analogue without a β substituent and therefore a possible substrate". In aqueous solution, most of the HC-3 will be present as a hemi-acetal, and therefore, the K_M for the actual substrate—the seco form of HC-3—is likely much smaller than the measured K_M, which incorporates the nonactive hemi-acetal form. On this basis, the seco form of HC-3 appears to be an exceedingly good substrate, perhaps even better than choline. Interestingly, the distance between the two phenyl rings of HC-3 has a striking effect on the ability of ChAT to catalyze the acetylation of HC-3 analogues; the insertion of one, two, or four methylene groups between the two phenyl rings of HC-3 decreases the rate of acetylation of the compound approximately 10-fold, but insertion of three methylene groups has no effect (*32*). These results show that the active site tunnel imparts specificity for extended N-linked substituents of choline analogues.

CoA and Acetyl-CoA Binding. To map ChAT−CoA interactions, CoA was soaked into crystals of unliganded ChAT, and data were collected to a resolution of 2.3 Å (Table 1), providing good difference electron density for the entire CoA molecule (Figure 4A). Most of the interactions with CoA are mediated by the binding domain of ChAT. The pyrophosphate and 3′-phosphoadenosine moieties lie on the surface of a shallow and open groove on the binding domain (Figure 4A). The positively charged side chains of K403 and K407 interact directly with the negatively charged 3′-phosphate of CoA (Figure 4B), and although the substrate-binding tunnel has a neutral or negative electrostatic potential, the surface surrounding the tunnel entrance for CoA has a relatively strong positive electrostatic potential (Figure 4A). The pantotheine is bound more deeply in the tunnel, cradled between the two splayed β-strands, which are a hallmark feature of this family of acetyltransferases. The separation of the β-strands exposes main chain amides that form

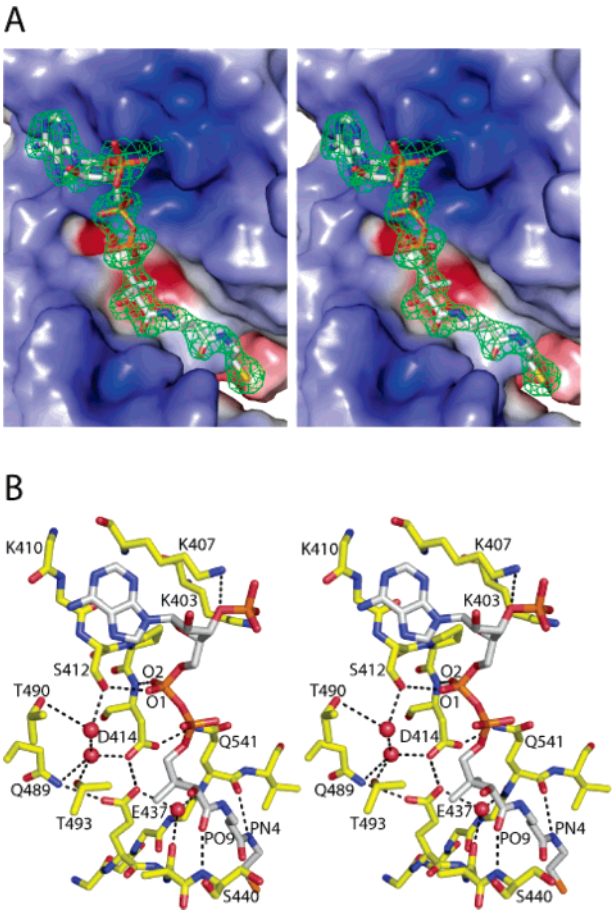

FIGURE 4: The CoA binding site of HChAT. (A) The molecular surface of the binding domain is shown, along with the bound CoA and the initial difference electron density map for CoA (green mesh). (B) Stereo diagram showing hydrogen-bonding interactions in the CoA binding site of ChAT. The CoA molecule forms five hydrogen bonds with the enzyme: two occur between pantotheine amide atoms PO9 or PN4 and ChAT main chain amide atoms, at either S440 or Q541; two other hydrogen bonds are between pyrophosphate oxygens O1 and O2 and S412 or D141, respectively; and the fifth is between the 3′-phosphate and the side chain of K407. The pyrophosphate moiety sits above the two closely interacting carboxylic acid side chains of D414 and E437. Because there are no formal positive charges in the vicinity of these side chains, they impart a negative electrostatic potential to the region.

hydrogen bonds with the pantotheine amides of CoA, locking the CoA sulfur atom into position in the active site (Figure 4B). Additional hydrogen bonds between ChAT and CoA are formed by O1 and O2 of the pyrophosphate moiety as well as the 3′-phosphate of CoA.

An interesting feature of the CoA binding surface is a region of negative electrostatic potential that forms the binding site for the two methyl groups of the pantotheine arm (Figure 4). The negative surface potential is generated by two acidic groups, D414 and E437, whose carboxylates come in close contact such that the two side chain oxygens have an interatomic distance of less than 2.6 Å and likely share a proton (*33*), resulting in a combined charge of −1 at physiological pH; this is supported by a theoretical p*K*a value of 11.8 for the side chain of E437. Although there are no positive compensating charges in the vicinity, each carboxylate accepts a hydrogen bond from a flanking glutamine, either Q489 or Q541, with an additional hydrogen bond donated to the side chain of D414 by a water molecule. Closely associated acidic residues are not uncommon in

proteins (*33*, *34*), but it is surprising to find them involved in binding two neutral methyl groups. In fact, it may be that the function of D414 and E437 is not to actively bind the methyl groups but instead to to repel the negatively charged pyrophosphate moiety so that the CoA molecule is forced to bind in only one manner.

Acetyl-CoA was also soaked into unliganded crystals of ChAT, but electron density for the acetyl moiety was always weak or nonexistent in *Fo*−*Fc* difference maps, indicating that acetyl-CoA can be hydrolyzed when it is bound to the enzyme. To help position the acetyl group of acetyl-CoA in the active site, we synthesized a stable analogue of acetyl-CoA, *S*-(2-oxopropyl)-CoA, and determined that this compound is a competitive inhibitor of ChAT with a K_i of 2.8 μM, which is similar to the K_m for acetyl-CoA (3.8 μM). The difference between *S*-(2-oxopropyl)-CoA and acetyl-CoA is in a methylene group that separates the CoA sulfur from the carbonyl carbon of the acetyl group. Crystals of unliganded ChAT were soaked in a solution containing *S*-(2-oxopropyl)-CoA to obtain a dataset for the complex (Table 1). In the structure of the complex, the 3′-phosphoadenosine, pyrophosphate, and pantotheine moieties of *S*-(2-oxopropyl)-CoA were bound in the same manner as CoA. The position of the sulfur atom was confirmed by the presence of a peak in the anomalous difference electron density map and was the same as that of the sulfur atom in bound CoA (Figure 5A). The 2-oxopropyl group attached to the sulfur was positioned inside the difference electron density, with the carbonyl oxygen positioned to form a hydrogen bond with the sulfhydryl of C550.

To build a model for acetyl-CoA using the *S*-(2-oxopropyl)-CoA structure, the carbonyl carbon of acetyl-CoA was placed at the position of the 2-oxopropyl methylene carbon (Figure 5). The acetyl group was then rotated around the S−C bond so that the carbonyl oxygen could form a hydrogen bond with the side chain oxygen of S540. In this position, the thioester in the ChAT/acetyl-CoA model fits well with the position of bound choline that was obtained from the ChAT/choline binary complex.

Structure-Based Model for Acetylcholine Synthesis. The binary ChAT/acetyl-CoA and ChAT/choline complexes were used together to obtain a model for the ternary Michaelis complex between ChAT, acetyl-CoA, and choline (Figure 5B). In this model, the carbonyl carbon of the acetyl group is positioned approximately 2 Å from the oxygen of bound choline, which is in turn hydrogen bonded to the catalytic histidine, H324. Thus, the choline oxygen atom is poised for nucleophilic attack on the carbonyl carbon of the thioester. The carbonyl oxygen of the thioester is hydrogen bonded to S540, which likely functions to support the developing negative charge.

The relative positions of the acetyl-CoA thioester substrate and the catalytic machinery, base, nucleophile, and oxyanion ligand, resemble what is found in serine endoproteases, which use a similar chemistry to effect amide hydrolysis and formation of an acyl−enzyme intermediate. The relationship can be illustrated by comparing the ChAT ternary Michaelis complex with the trypsin−BPTI complex (*35*) in which BPTI provides a good model for bound substrate (Figure 5C). By superposing the two scissile ester bonds, the thioester of acetyl CoA and the amide ester of BPTI, the relationship between the catalytic elements can be seen. In each case, the nucleophile, either the side chain of S195 in the case of trypsin or the hydroxyl group of bound choline in the case of ChAT, is positioned directly below the carbonyl carbon of the ester substrate, with a general base, namely, an imidazole nitrogen, approximately 2.8 Å away. The overall

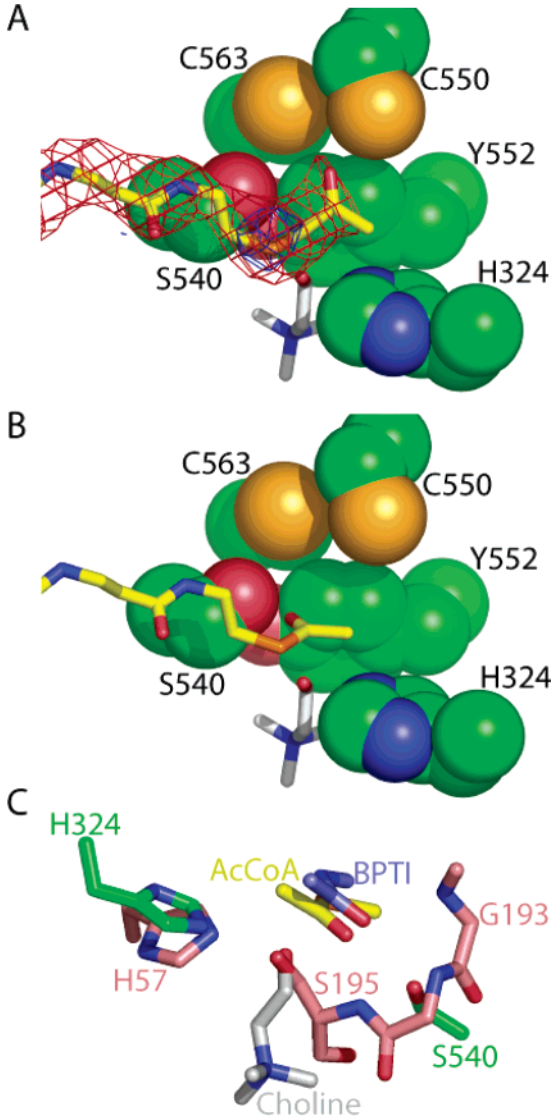

FIGURE 5: Active site chemistry in HChAT. (A) The structure of ChAT in complex with a stable acetyl-CoA analogue, *S*-(2-oxopropyl)-CoA, was determined. Difference Fourier electron density, (red mesh, contoured at 2σ) and anomalous difference electron density (blue mesh, contoured at 3σ) are shown along with the pantotheine arm of the *S*-(2-oxopropyl)-CoA molecule; the oxopropyl group was used to help position the acetyl group in a model of the ChAT−[acetyl-CoA] complex. Note that the choline molecule present in this panel was not part of the crystallographic structure but has been modeled on the basis of its position in the ChAT−choline binary complex. (B) A model for the active ternary complex based on the two binary complexes of ChAT−choline and ChAT−[*S*-(2-oxopropyl)-CoA]. To model acetyl-CoA, the acetyl group was positioned such that the carbonyl carbon occupies the same position as the oxopropyl methylene group in the ChAT−[*S*-(2-oxopropyl)-CoA] structure; rotation about the S−C bond allows the carbonyl oxygen to hydrogen bond with the side chain of S540. Choline has been placed such that its position is identical to that in the structure of the ChAT−choline binary complex. (C) HChAT uses the same chemistry as the serine endoproteases to effect ester hydrolysis. In this panel, the active site elements of trypsin (pink carbon atoms) and the scissile bond of pancreatic trypsin inhibitor (BPTI; blue carbon atoms) are superimposed with the ChAT−choline−[acetyl-CoA] ternary complex.

geometry of the base, nucleophile, and substrate is almost identical in the two complexes. In trypsin, the negative charge on the transition state oxyanion is supported by two main-chain amide groups, one from S195 and the second from G193, which are positioned to form geometrically ideal hydrogen bonds with the oxyanion. In the ChAT Michaelis complex, the side chain hydroxyl of S540 is 3 Å from the carbonyl oxygen of acetyl-CoA, and is found in the same relative area as the oxyanion hole in trypsin (Figure 5C). Thus, by analogy with trypsin, the position of S540 relative to that of the nucleophile, substrate, and catalytic base supports its role as an oxyanion ligand. The only other potential hydrogen-bonding partners for the oxyanion are the thiols of C550 and C563; however, both thiols are 5 Å away from the carbonyl oxygen of acetyl-CoA, and neither is in a good position to donate a hydrogen bond.

Conformational Changes Accompanying CoA Binding. Binding of CoA leads to conformational changes in hChAT that can be visualized if the binding domains of the unliganded and CoA-bound enzymes are superposed (Figure 6A). The catalytic domain is rotated approximately 1.5° about an axis that runs through the active site of the enzyme. Figure 6B shows the CA displacements for this conformational change, where it can be seen that a similar conformational change took place in the complex between ChAT and *S*-(2-oxopropyl)-CoA but was not observed in the ChAT−choline complex. Thus, CoA binding is causing a small but significant domain movement.

An important structural change occurs in a P-loop, which helps to bind CoA. In the case of the unliganded protein, there was no electron density for P-loop residues 139 to 146, indicating that the loop was mobile. In the ChAT−CoA complex, electron density for residues 139 to 146 indicated that the loop lies across the surface of the binding domain (Figure 6A) such that residues 142 to 144 interact directly with the phosphates of bound CoA (Figure 6C); the interaction consists of two hydrogen bonds from the main chain and side chain amides of Q44 to pyrophosphate oxygens O1 and O4. In addition, the side chain of K142 is close enough (5−8 Å) to the 3′-phosphate that its positive charge would contribute to the P-loop/CoA interaction. Thus, the CoA binding site is formed primarily from residues on the binding domain, but residues 139 to 148 on the catalytic domain, the P-loop, reach across the active site tunnel to interact with phosphoadenosine of either CoA or acetyl-CoA.

Cai and co-workers cocrystallized rat ChAT (rChAT) with CoA and obtained data to 3.7 Å resolution (*23*). In the resulting rChAT-CoA structure, domain movements and/or a change in the position of the P-loop were not reported; however, the low resolution of the data precluded refinement of the structure, and coordinates were not deposited in the Protein Data Bank. Interestingly, in the two published structures of unliganded rChAT, the P-loop was well-localized (*23*, *24*); however, in both cases, the P-loop participates in a crystal contact, and therefore its location and conformation are probably not representative of the structure in solution. In fact, the conformation of the P-loop is different in the two rChAT structures (the outermost residues of the loop are displaced more than 10 Å), supporting the notion that the loop is conformationally flexible in solution, and its position in the unliganded rChAT structures is determined by crystal-packing forces.

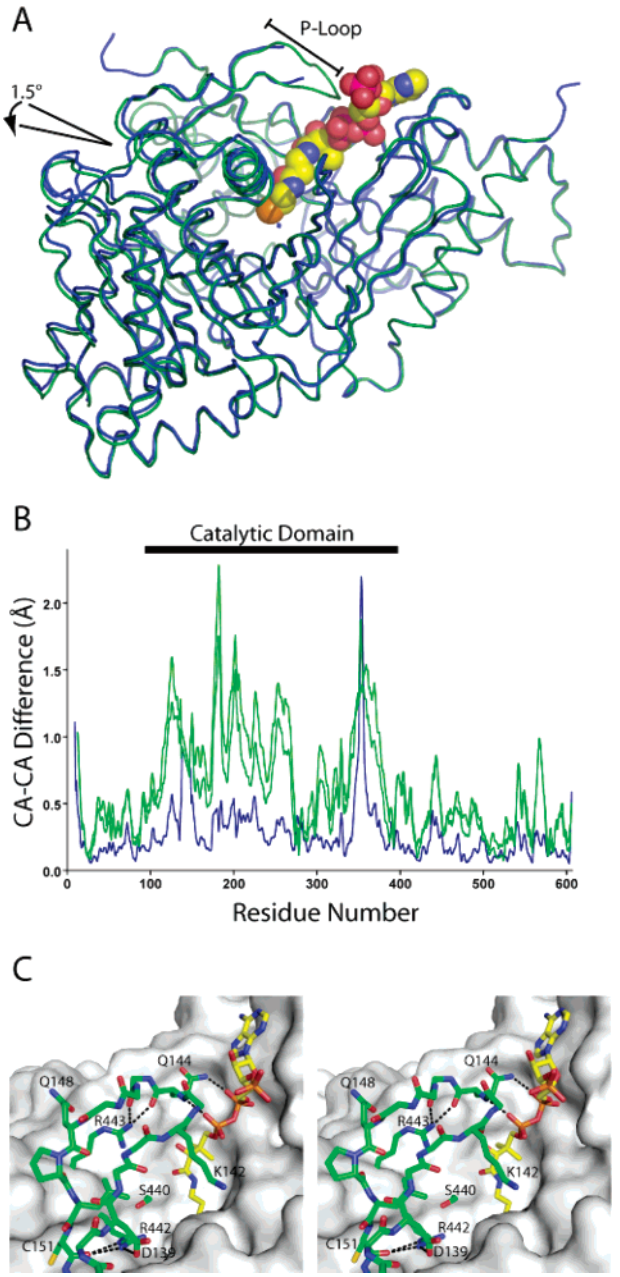

FIGURE 6: CoA-induced conformational changes in ChAT. (A) To illustrate the domain movements that occur in ChAT upon ligand binding, the binding domain of apo-ChAT (blue) was superposed on the binding domain of CoA-bound ChAT (green); the conformational change accompanying CoA binding involves a 1.5° rotation of the catalytic domain relative to the binding domain and an anchoring of the P-loop such that it interacts with the phosphates of the bound CoA. (B) A plot of CA differences between the unliganded ChAT structure and each of the three complexes. To generate this plot, CA−CA distances were calculated after the binding domain of unliganded ChAT was superposed over that of either ChAT−choline (blue), ChAT-CoA (dark green), or ChAT−[*S*-(2-oxopropyl)-CoA] (light green). The residues corresponding to the catalytic domain are indicated by the bar above the plot. (C) Residue Q144 of the P-loop (green carbon atoms) forms hydrogen bonds with two of the CoA pyrophosphate oxygens. The P-loop also interacts with the side chains of R442 and R443. The side chain of S440 is a site of phosphorylation (*41*).

ChAT is unique in that the P-loop is not present in other members of the family, such as carnitine acetyltransferase (CrAT), chloramphenicol acetyltransferase, or dihydrolipoyl transacetylase (*26*, *36*, *37*). In particular, the CoA binding site of human CrAT (*26*) is very similar to that of hChAT,

and the extended P-loop in ChAT is one difference that could explain its 10-fold lower K_M for CoA compared with that of CrAT (*16*, *38*), a possibility that was raised when the structure of rChAT was solved (*23*). The difference in K_M likely reflects requirements imposed on the enzymes by their cellular locations. ChAT resides in the cytosolic compartment in which the acetyl-CoA concentration has been estimated to be 3.5−10.9 μM, whereas CrAT is located in the mitochondria (*39*), where the acetyl-CoA concentration is thought to be much higher (*40*). Thus, by increasing the affinity of the enzyme for acetyl-CoA, the P-loop in hChAT may enable it to more efficiently use the lower concentrations of acetyl-CoA found in the cytosol.

There is evidence that CoA binding and the interaction between the P-loop and CoA are important for ChAT function and regulation *in vivo*. In studies of the rat enzyme, R442 and R443 were shown to be important for CoA binding. A double mutant, R442Q/R443Q, had K_M for CoA over 100-fold greater than that of the wild-type enzyme, along with an 18-fold greater k_{cat}, consistent with CoA release being the rate-limiting step in acetylcholine synthesis (*20*). The effect of mutations at R442 and R443 were much less pronounced when dephospho-CoA was used in the kinetic analysis, suggesting that these arginine residues were important for binding the 3′-phosphate of CoA. These points were raised in the article describing the rChAT-CoA structure (*23*), prompting the authors to speculate that the 3′-phosphate might bind directly to R442 and R443, although the structure of their complex indicated that this was not the case. The structure of CoA-bound hChAT confirms that R442 and R443 do not bind directly to the 3′-phosphate group, but they do form multiple interactions with P-loop residues. To be specific, R442 interacts with the side chain of D139 and the main chain carbonyl oxygen of C151, whereas R443 hydrogen bonds to the main chain oxygens of Q144 and L145. Regarding R442 and the function of hChAT, it is noteworthy that the mutation to histidine was found in a patient with episodic apnea, and *in vitro*, the R442H enzyme had a markedly increased K_M for acetyl-CoA (*3*). Thus, the mutagenic data for R442 and R443 support the idea that the interaction of the P-loop with bound CoA is critical for the enzyme's catalytic properties and *in vivo* function.

CoA binding and the subcellular localization of ChAT appear to be regulated by phosphorylation, and one of the sites phosphorylated *in vivo* was identified as S440 (*41*), which is in the CoA binding site in the region of the P-loop (Figure 6C). Phosphorylation of hChAT by PKC *in vitro* led to a 2-fold increase in its catalytic activity (*42*), and the activity of the 69 kDa form of hChAT in HEK293 cells was increased 1.6-fold by treatment with phorbol 12-myristate 13-acetate, an activator of PKC. The mutation of S440 to alanine resulted in a pronounced decrease in overall phosphorylation of ChAT, an attenuation of the PKC-mediated increase in activity, and a loss of membrane binding of ChAT *in situ* (*41*). These results suggest that the phosphorylation state of S440 has a role in coordinating key functions of the enzyme.

CONCLUSION

The structure of hChAT in complex with CoA shows that a P-loop, which is disordered in the unliganded protein, interacts with the phosphates of CoA. This loop is 4 residues shorter in CrAT, and as such, it cannot interact with CoA; a comparison of the CoA-bound structures of these two related enzymes shows that the P-loop is responsible for the lower K_M of hChAT, which allows it to be optimally active under the lower concentration of acetyl-CoA in the cytosol. ChAT and CrAT differ in that the well-characterized effect of salts on the activity of ChAT (high ionic strength raises both the K_M and V_{max} of the enzyme (*21*, *22*)) has not been documented for CrAT. Thus, the P-loop in hChAT is most likely responsible for the effects of salts on the catalytic activity of the enzyme, consistent with the hChAT-CoA structure showing that interactions between the P-loop and CoA are electrostatic in nature. Serine 440 is a major site of phosphorylation of hChAT (*41*), and its presence in the vicinity of the P-loop is noteworthy. A phosphate group on S440 could interfere directly with CoA binding (*23*), or it could interfere indirectly by competing with the P-loop for interaction with R442 and R443 (Figure 6C). In either case, phosphorylation would be expected to raise the K_M for acetyl-CoA. The higher K_M would increase the V_{max} *in vitro*, but *in vivo*, the activity of the enzyme would be expected to decrease with the relatively low acetyl-CoA concentration in the cytosol.

The hChAT−choline complex explains how a variety of substrates can be acetylated by the enzyme. It is particularly interesting that homocholine is not a substrate for the soluble enzyme but can be acetylated by membrane-bound ChAT (*29*). The structure of the choline binding site shows that there may be a conformational change in the enzyme, most likely involving movement of residues 84 and 85, that allows it to bind and acetylate homocholine. It is possible that a change in the position of residues 84 and 85 takes place when ChAT binds to membranes. These residues are not part of an inflexible domain core but instead are part of the polypeptide that connects the binding domain with the catalytic domain. On this basis, it is not inconceivable that residues 84 and 85 could shift under certain conditions.

Regulation of ChAT activity may take place *in vivo*, perhaps to ensure that acetylcholine synthesis is efficiently coupled to choline uptake and acetylcholine transport at synaptic vesicles. ChAT is phosphorylated on at least six residues (*41*, *43*, *44*), and phosphorylation of ChAT appears to alter its catalytic activity and subcellular localization (*41*) and may regulate its interaction with other proteins (*43*), all of which could regulate acetylcholine production and affect cholinergic neurotransmission. Future studies should focus on the mechanisms by which ChAT is compartmentalized within the nerve terminal and the structural factors modulating its association with cellular membranes and acquisition of choline from CHT1.

MATERIALS AND METHODS

Crystallization and Data Collection. Recombinant hChAT, with surface mutations designed to improve crystallization, was expressed, purified, and crystallized as previously described (*25*, *27*). Appropriate residues for mutation were located using the rChAT structure (*23*) as a model for hChAT. Three turns that project glutamyl and/or lysyl side chains away from the surface of the enzyme were identified, and the residues in these turns were mutated to alanine on

the basis of the prediction that they would form good crystal contacts (*45*). The three sets of mutations were E225A/D226A/E227A, K518A/E519A, and K582A/E583A. In addition to these changes, a loop region in ChAT was also altered. The loop in question comprises residues 346 to 358 and was found to be highly mobile and disordered in the rChAT structure (*23*); however, the corresponding loop was relatively well-ordered in the structure carnitine acetyltransferase (CrAT), a closely related enzyme (*26*). Therefore, residues 346 to 358 in hChAT were replaced with the sequence PELVRSPMVP from human CrAT, shortening the loop by three residues. Finally, the last 15 amino acids of ChAT, residues 615 to 630, were deleted because they are prone to proteolysis and likely disordered (*27*). None of the changes had a significant effect on the catalytic activity of the enzyme (*25*).

For the ChAT−choline complex, the protein was cocrystallized with 10 mM acetylcholine. Crystals of unliganded ChAT or the ChAT−choline complex were cryoprotected in crystallization mother liquor containing 30% glycerol and flash frozen in liquid nitrogen. Complexes between ChAT and CoA or *S*-(2-oxopropyl)-CoA were obtained by soaking crystals of the unliganded protein in mother liquor supplemented with 0.1 mM tris(2-carboxyethyl)phosphine (TCEP) and either 20 mM CoA or *S*-(2-oxopropyl)-CoA for 5 h or 75 min, respectively, at 4 °C. The ChAT-CoA crystals were transferred to a solution containing 20% PEG 2000 monomethyl ether, 10% glycerol, 20 mM CoA, and 0.1 M Tris at pH 8.5−9 for cryoprotection, briefly before being flash-frozen. The cryoprotection solution for ChAT-*S*-(2-oxopropyl)-CoA crystals was 30% PEG 3350, 10% glycerol, 0.5 mM TCEP, and 20 mM *S*-(2-oxopropyl)-CoA. Diffraction data for human unliganded ChAT as well as the CoA and *S*-(2-oxopropyl)-CoA complexes were collected in-house using a Rigaku RUH3R rotating anode X-ray generator (λ = 1.5418 Å) with a MAR345 image plate detector. Data from ChAT-CoA crystals were collected at the National Synchrotron Light Source (NSLS) beamline X8C (λ = 1.1 Å) using an ADSC Quantum 4R CCD detector system, with a crystal-to-detector distance of 150 mm and an oscillation angle of 1°. In all cases, the images were indexed, processed, and merged using the HKL suite (*46*).

Structure Determination and Refinement. The structure of unliganded hChAT was solved by molecular replacement using the coordinates of rChAT (*23*; pdb accession code 1Q6X) and the program AMoRe (*47*). Refinement was initiated by rigid body fitting, followed by simulated annealing, energy minimization, grouped B-factor refinement, and, finally, individual B-factor refinement within CNS (*48*). The R_{free} value was monitored throughout refinement using 10% of randomly selected reflections. Subsequent rounds of refinement were done by manual rebuilding and water placement using O (*49*), followed by energy minimization and B-factor refinement in CNS. The final structure was validated with PROCHECK (*50*), and in the final model, all residues were found in favored regions of the Ramachandran plot except for V94 (ϕ = 68.6, ψ = −49.7), which is in a type II turn in the vicinity of the active site. Regions for which electron density was not observed, namely residues 1 to 7, 139 to 146, 176 to 179, and 608 to 615, were not included in the model of unliganded ChAT.

The refined structure of unliganded hChAT was used to calculate difference electron density maps for the three complexes; in each case, there was clear electron density for the ligand, choline, CoA, or *S*-(2-oxopropyl)-CoA. In the case of the CoA-bound structures, the initial rigid body refinement was improved by dividing the protein into two domains, the binding domain, residues 1 to 89 and 392 to 615, and the catalytic domain, residues 90 to 391. For both of the CoA structures, highly redundant datasets were collected, and anomalous difference electron density maps were used to confirm the position of the sulfur atoms in the ligands. All Figures were created using PyMol (DeLano Scientific LLC; http://pymol.sourceforge.net/), and surface potentials were calculated using the program APBS (*51*). Note that the surfaces displayed are molecular surfaces, which allows the visualization of bound ligands, but the potentials correspond to those found on the solvent-accessible surface. Theoretical p*K*a values were calculated using the PROPKA server (http://propka.chem.uiowa.edu; *52*).

Synthesis of S-(2-Oxopropyl)-CoA and ChAT Inhibition. The synthesis and purification of *S*-(2-oxopropyl)-CoA were monitored by silica gel TLC developed in propanol/methanol/water = 4:3:2; *S*-(2-oxopropyl)-CoA migrates with an R_f of 0.65 under these conditions. To synthesize the compound, CoA trilithium salt (100 mg or 0.127 mmol; Sigma) was dissolved in 5 mL of degassed water. While stirring under a nitrogen atmosphere, 0.04 mmol of DTT and 0.81 mmol of Li_2CO_3 were added. Chloroacetone (0.37 mmol; Aldrich) in 12 mL of 95% ethanol was added to the above mixture, and the resulting turbid solution was stirred at room temperature for 24 h. The solution was then filtered and concentrated *in vacuo* to give a yellow film. The film was dissolved in water and was purified by reverse-phase HPLC (Symmetry 300 C18, Waters). The amount of *S*-(2-oxopropyl)-CoA obtained was 38 mg, corresponding to an overall yield of 36%. A molecular weight of 823.33 g/mol was determined for the purified compound by mass spectrometry (theoretical MW 823.61 g/mol).

To characterize the inhibition of ChAT activity by *S*-(2-oxopropyl)-CoA, a modification (*53*) of the radio-enzymatic assay of Fonnum (*54*) was used. ChAT was diluted with 10 mM Na_2HPO_4, 1 mM EDTA, 0.5% Triton, 150 mM NaCl, 0.05% BSA, and 0.5 mM TCEP at pH 7.5 to give a final concentration of 1.3 μg/L. The reaction was initiated by the addition of 10 μL of the diluted ChAT solution to 10 μL of the reaction mixture comprised of 50 mM Na_2HPO_4, 150 mM NaCl, 0.05% BSA, 0.5 mM TCEP, 10 mM choline at pH 7.5, along with varying amounts of [^{3}H]acetyl-CoA and *S*-(2-oxopropyl)-CoA. The reaction was allowed to proceed at 37 °C for 10 min and then stopped by the addition of 100 μL of cold water; note that during the 10 min reaction course, product formation increased in a linear fashion, as expected for an initial rate measurement. To extract [^{3}H]acetylcholine, 300 μL of 20 mg/mL sodium tetraphenylboron in 3-heptanone was added, and the samples were vortexed for 30 s and centrifuged at 7000*g* for 5 min. The [^{3}H]acetylcholine contained in 200 μL of the organic phase was measured by liquid scintillation spectrometry; samples were normalized for protein content and incubation time to yield activity units of μmol of acetylcholine/min/mg.

ACKNOWLEDGMENT

We thank Stan Dunn for useful discussions.

REFERENCES

1. Whitehouse, P. J. (1998) The cholinergic deficit in Alzheimer's disease, *J. Clin. Psychiatry 59*, 19−22.
2. Holt, D. J., Bachus, S. E., Hyde, T. M., Wittie, M., Herman, M. M., Vangel, M., Saper, C. B., and Kleinman, J. E. (2005) Reduced density of cholinergic interneurons in the ventral striatum in schizophrenia: an in situ hybridization study, *Biol. Psychiatry 58*, 408−416.
3. Ohno, K., Tsujino, A., Brengman, J. M., Harper, C. M., Bajzer, Z., Udd, B., Beyring, R., Robb, S., Kirkham, F. J., and Engel, A. G. (2001) Choline acetyltransferase mutations cause myasthenic syndrome associated with episodic apnea in humans, *Proc. Natl. Acad. Sci. U.S.A. 98*, 2017−2022.
4. Kawashima, K., and Fujii, T. (2003) The lymphocytic cholinergic system and its biological function, *Life Sci. 72*, 2101−2109.
5. Hersh, L. B., and Peet, M. (1978) Effect of salts on the physical and kinetic properties of human placental choline acetyltransferase, *J. Neurochem. 30*, 1087−1093.
6. Gill, S. K., Bhattacharya, M., Ferguson, S. S., and Rylett, R. J. (2003) Identification of a novel nuclear localization signal common to 69- and 82-kDa human choline acetyltransferase, *J. Biol. Chem. 278*, 20217−20224.
7. Resendes, M. C., Dobransky, T., Ferguson, S. S., and Rylett, R. J. (1999) Nuclear localization of the 82-kDa form of human choline acetyltransferase, *J. Biol. Chem. 274*, 19417−19421.
8. Gill, S. K., Ishak, M., and Rylett, R. J. (2005) Exposure of nuclear antigens in formalin-fixed, paraffin-embedded necropsy human spinal cord tissue: detection of NeuN, *J. Neurosci. Methods 148*, 26−35.
9. Varoqui, H., and Erickson, J. D. (1996) Active transport of acetylcholine by the human vesicular acetylcholine transporter, *J. Biol. Chem. 271*, 27229−27232.
10. Weiler, M. H., Gundersen, C. B., and Jenden, D. J. (1981) Choline uptake and acetylcholine synthesis in synaptosomes: investigations using two different labeled variants of choline, *J. Neurochem. 36*, 1802−1812.
11. Okuda, T., Haga, T., Kanai, Y., Endou, H., Ishihara, T., and Katsura, I. (2000) Identification and characterization of the high-affinity choline transporter, *Nat. Neurosci. 3*, 120−125.
12. Gabrielle, P., Jeana, M., and Lorenza, E. C. (2003) Cytosolic choline acetyltransferase binds specifically to cholinergic plasma membrane of rat brain synaptosomes to generate membrane-bound enzyme, *Neurochem. Res. 28*, 543−549.
13. Nakata, K., Okuda, T., and Misawa, H. (2004) Ultrastructural localization of high-affinity choline transporter in the rat neuromuscular junction: enrichment on synaptic vesicles, *Synapse 53*, 53−56.
14. Dobransky, T., and Rylett, R. J. (2005) A model for dynamic regulation of choline acetyltransferase by phosphorylation, *J. Neurochem. 95*, 305−313.
15. Murzin, A. G., Brenner, S. E., Hubbard, T., and Chothia, C. (1995) SCOP: a structural classification of proteins database for the investigation of sequences and structures, *J. Mol. Biol. 247*, 536−540.
16. Hersh, L. B., and Peet, M. (1977) Re-evaluation of the kinetic mechanism of the choline acetyltransferase reaction, *J. Biol. Chem. 252*, 4796−4802.
17. Carbini, L. A., and Hersh, L. B. (1993) Functional analysis of conserved histidines in choline acetyltransferase by site-directed mutagenesis, *J. Neurochem. 61*, 247−253.
18. Hersh, L. B., Nair, R. V., and Smith, D. J. (1979) The reaction of choline acetyltransferase with sulfhydryl reagents. Methoxycarbonyl-CoA disulfide as an active site-directed reagent, *J. Biol. Chem. 254*, 11988−11992.
19. Carbini, L., Rodriguez, G., and Hersh, L. B. (1990) Kinetic and inactivation studies of recombinant Drosophila choline acetyltransferase, *Brain Res. Bull. 24*, 119−124.
20. Wu, D., and Hersh, L. B. (1995) Identification of an active site arginine in rat choline acetyltransferase by alanine scanning mutagenesis, *J. Biol. Chem. 270*, 29111−29116.
21. Hersh, L. B. (1979) The lack of specificity towards salts in the activation of choline acetyltransferase from human placenta, *J. Neurochem. 32*, 991−996.
22. Hersh, L. B., Barker, L. A., and Rush, B. (1978) Effect of sodium chloride on changing the rate-limiting step in the human placental choline acetyltransferase reaction, *J. Biol. Chem. 253*, 4966−4970.
23. Cai, Y., Cronin, C. N., Engel, A. G., Ohno, K., Hersh, L. B., and Rodgers, D. W. (2004) Choline acetyltransferase structure reveals distribution of mutations that cause motor disorders, *EMBO J. 23*, 2047−2058.
24. Govindasamy, L., Pedersen, B., Lian, W., Kukar, T., Gu, Y., Jin, S., Agbandje-McKenna, M., Wu, D., and McKenna, R. (2004) Structural insights and functional implications of choline acetyltransferase, *J. Struct. Biol. 148*, 226−235.
25. Kim, A. R., Dobransky, T., Rylett, R. J., and Shilton, B. H. (2005) Surface-entropy reduction used in the crystallization of human choline acetyltransferase, *Acta Crystallogr., Sect. D 61*, 1306−1310.
26. Jogl, G., and Tong, L. (2003) Crystal structure of carnitine acetyltransferase and implications for the catalytic mechanism and fatty acid transport, *Cell 112*, 113−122.
27. Kim, A. R., Doherty-Kirby, A., Lajoie, G., Rylett, R. J., and Shilton, B. H. (2005) Two methods for large-scale purification of recombinant human choline acetyltransferase, *Protein Expression Purif. 40*, 107−117.
28. Barker, L. A., and Mittag, T. W. (1975) Comparative studies of substrates and inhibitors of choline transport and choline acetyltransferase, *J. Pharmacol. Exp. Ther. 192*, 86−94.
29. Benishin, C. G., and Carroll, P. T. (1981) Acetylation of choline and homocholine by membrane-bound choline-O-acetyltransferase in mouse forebrain nerve endings, *J. Neurochem. 36*, 732−740.
30. Hemsworth, B. A., Shreeve, S. M., and Veitch, G. B. (1984) Pharmacological actions of some cyclic analogues of choline, *Br. J. Pharmacol. 81*, 685−692.
31. Welner, S. A., and Collier, B. (1984) Uptake, metabolism, and releasability of ethyl analogues of homocholine by rat brain, *J. Neurochem. 43*, 1143−1151.
32. Shreeve, S. M., Veitch, G. B., and Hemsworth, B. A. (1984) Acetylation of some novel hemicholinium compounds by soluble choline acetyltransferase: structure−activity relationships, *J. Med. Chem. 27*, 754−757.
33. Torshin, I. Y., Harrison, R. W., and Weber, I. T. (2003) Close pairs of carboxylates: a possibility of multicenter hydrogen bonds in proteins, *Protein Eng. 16*, 201−207.
34. Flocco, M. M., and Mowbray, S. L. (1995) Strange bedfellows: interactions between acidic side-chains in proteins, *J. Mol. Biol. 254*, 96−105.
35. Huber, R., Kukla, D., Bode, W., Schwager, P., Bartels, K., Deisenhofer, J., and Steigemann, W. (1974) Structure of the complex formed by bovine trypsin and bovine pancreatic trypsin inhibitor. II. Crystallographic refinement at 1.9 A resolution, *J. Mol. Biol. 89*, 73−101.
36. Leslie, A. G., Moody, P. C., and Shaw, W. V. (1988) Structure of chloramphenicol acetyltransferase at 1.75-A resolution, *Proc. Natl. Acad. Sci. U.S.A. 85*, 4133−4137.
37. Mattevi, A., Obmolova, G., Kalk, K. H., Teplyakov, A., and Hol, W. G. (1993) Crystallographic analysis of substrate binding and catalysis in dihydrolipoyl transacetylase (E2p), *Biochemistry 32*, 3887−3901.
38. Bloisi, W., Colombo, I., Garavaglia, B., Giardini, R., Finocchiaro, G., and Didonato, S. (1990) Purification and properties of carnitine acetyltransferase from human liver, *Eur. J. Biochem. 189*, 539−546.
39. Zammit, V. A. (1999) Carnitine acyltransferases: functional significance of subcellular distribution and membrane topology, *Prog. Lipid Res. 38*, 199−224.
40. Leonardi, R., Zhang, Y. M., Rock, C. O., and Jackowski, S. (2005) Coenzyme A: back in action, *Prog. Lipid Res. 44*, 125−153.
41. Dobransky, T., Davis, W. L., and Rylett, R. J. (2001) Functional characterization of phosphorylation of 69-kDa human choline acetyltransferase at serine 440 by protein kinase C, *J. Biol. Chem. 276*, 22244−22250.
42. Dobransky, T., Davis, W. L., Xiao, G. H., and Rylett, R. J. (2000) Expression, purification and characterization of recombinant human choline acetyltransferase: phosphorylation of the enzyme regulates catalytic activity, *Biochem. J. 349*, 141−151.
43. Dobransky, T., Brewer, D., Lajoie, G., and Rylett, R. J. (2003) Phosphorylation of 69-kDa choline acetyltransferase at threonine 456 in response to amyloid-beta peptide 1-42, *J. Biol. Chem. 278*, 5883−5893.
44. Dobransky, T., Doherty-Kirby, A., Kim, A. R., Brewer, D., Lajoie, G., and Rylett, R. J. (2004) Protein kinase-C isoforms differentially

phosphorylate human choline acetyltransferase regulating its catalytic activity, *J. Biol. Chem. 279*, 52059−52068.
45. Derewenda, Z. S. (2004) Rational protein crystallization by mutational surface engineering, *Structure 12*, 529−535.
46. Otwinowski, Z., and Minor, W. (1997) Processing of X-ray diffraction data collected in oscillation mode, *Methods Enzymol. 276*, 307−326.
47. Navaza, J. (1994) AMoRe: an automated package for molecular replacement, *Acta Crystallogr. Sect. A 50*, 157−163.
48. Brünger, A. T., Adams, P. D., Clore, G. M., DeLano, W. L., Gros, P., Grosse-Kunstleve, R. W., Jiang, J. S., Kuszewski, J., Nilges, M., Pannu, N. S., Read, R. J., Rice, L. M., Simonson, T., and Warren, G. L. (1998) Crystallography & NMR system: A new software suite for macromolecular structure determination, *Acta Crystallogr., Sect. D 54*, 905−921.
49. Jones, T. A., Bergdoll, M., and Kjeldgaard, M. (1990) O: A Macromolecular Modeling Environment, in *Crystallographic and Modeling Methods in Molecular Design* (Bugg, C. E., and Ealick, S. E., Eds.) pp 189−195, Springer-Verlag: New York.
50. Laskowski, R. A., MacArthur, M. W., Moss, D. S., and Thornton, J. M. (1993) PROCHECK: a program to check the stereochemical quality of protein structures, *J. Appl. Crystallogr. 26*, 283−291.
51. Baker, N. A., Sept, D., Joseph, S., Holst, M. J., and McCammon, J. A. (2001) Electrostatics of nanosystems: application to microtubules and the ribosome, *Proc. Natl. Acad. Sci. U.S.A. 98*, 10037−10041.
52. Li, H., Robertson, A. D., and Jensen, J. H. (2005) Very fast empirical prediction and rationalization of protein pKa values, *Proteins 61*, 704−721.
53. Rylett, R. J., Goddard, S., and Lambros, A. (1993) Regulation of expression of cholinergic neuronal phenotypic markers in neuroblastoma LA-N-2, *J. Neurochem. 61*, 1388−1397.
54. Fonnum, F. (1975) A rapid radiochemical method for the determination of choline acetyltransferase, *J. Neurochem. 24*, 407−409.

BI061536L